IEEE Access
Multidisciplinary ⋮ Rapid Review ⋮ Open Access Journal

Received June 11, 2018, accepted July 15, 2018, date of publication July 27, 2018, date of current version September 21, 2018.

Digital Object Identifier 10.1109/ACCESS.2018.2857846

Stability Analysis With Considering the Transition Interval for PWM DC-DC Converters Based on Describing Function Method

HONG LI[1], (Senior Member, IEEE), JIANING SHANG[1], BO ZHANG[2], (Senior Member, IEEE), XINGRAN ZHAO[1], NANLIN TAN[3] AND CHEN LIU[1]

[1]School of Electrical Engineering, Beijing Jiaotong University, Beijing 100044, China
[2]School of Electric Power, South China University of Technology, Guangzhou 510640, China
[3]School of Mechanical Electronic and Control Engineering, Beijing Jiaotong University, Beijing 100044, China

Corresponding author: Hong Li (hli@bjtu.edu.cn)

This work was supported in part by the General Program of the National Natural Science Foundation of China under Grant 51577010, in part by the Fundamental Research Funds for the Central Universities under Grant 2017JBM054, and in part by the National Key Research and Development Program of China under Grant 2016YFE0131700.

ABSTRACT The nonlinearity of the switching process in DC–DC converters can result in the inaccuracy and invalidation of traditional stability criterion based on linear modeling, which is very harmful in practice, especially for the DC-DC converters with high stability requirements. In this paper, the describing function method is adopted for the modeling of switching process, namely, pulse width modulation (PWM), in DC–DC converters, and the describing function of the PWM is derived in detail. Considering the nonlinear items in the obtained describing function of PWM, the selection of the parameters in these nonlinear items are first provided and proved in this paper. With the obtained describing function, the stability of the PWM DC–DC converter can be analyzed exactly. Taken a PWM boost converter as an example, the nonlinear model based on describing function and the linear model are established, respectively; furthermore, the stability analysis based on these two kinds of models are carried out. Comparing with the traditional linear stability criterion, the simulation and experimental results validate the effectiveness and accuracy of the stability analysis based on describing function method. Furthermore, the transition interval of the PWM DC–DC converter from a stable region to an unstable region can be determined exactly by the proposed stability analysis method, which is helpful to determine the stability margin in real engineering applications. Therefore, this paper provides a practical stability analysis method for PWM DC–DC converters.

INDEX TERMS DC-DC converter, describing function, nonlinear modeling, stability analysis.

I. INTRODUCTION

As the most common and practical topology of the power converters, DC-DC converters have the advantages on simple structure, low cost and high conversion efficiency. DC-DC converters have been widely used in household appliances, electrical industries, aerospace and other fields [1]–[5]. Today, pulse width modulation (PWM) is widely adopted in DC-DC converters. In addition, the traditional linear modeling and stability analysis methods are usually used for DC-DC converters, such as the average state space method [6]. But as the rapid development of power electronic technologies, the requirements of power electronic systems or equipment on stability, reliability and electrical performance have become stricter and stricter. The traditional linear modeling and analysis methods more and more cannot satisfy these requirements due to the nonlinearity of power converters [7]. In recent decades, the nonlinear behaviors of the power converters have been gradually revealed [8], [9]. The application of nonlinear theories in the field of power electronics has become a hot topic and received wide attention both at home and abroad [10]–[14]. At present, the common nonlinear analysis methods include analytical method [15], [16], phase plane method [17], switch signal flow graph method [18], [19], describing function method [20], [21], etc. The analytical method solves the state-space averaged equations directly, which is suitable for the one or second-order system. But, the analytical method is very complicated for the high order systems [22]. The phase plane method is a graphic analysis method, and it transforms the movement of the first or second order system to a trajectory about position and velocity in phase plane, which is intuitive but also disabled for the high order systems [23]. The switch signal flow graph method is a nonlinear graphical modeling method, by which, the switching process can be equivalent as two linear branches in turn-on or turn-off periods [18], [19]. But the dedicated graphic computer simulation software is needed for the analysis. The three methods mentioned above all use the concept of averaging for system modeling and analysis, which can neither reflect the frequency characteristic of the nonlinear link nor be used in high order system.

Fortunately, Professor P. J. Daniel proposed describing function method in 1940, which is not only suitable for high order systems, but also can reflect the fundamental frequency characteristic of the nonlinear link. Therefore, it has been mainly used to analyze the stability of the systems with nonlinear link and self-oscillation problems in control domain. In recent years, the describing function method has been found and applied into electrical engineering [24]–[29]. In [24]–[26], the describing function method has been mentioned for modeling the whole system of power converter under frequency modulation. In [27], a two-rules fuzzy controller is modeled by describing function. In [28] and [29], the transfer functions of PWM link were deduced by describing function method, but only a few frequency components are considered. Until now, the describing function in power converters is mainly used for obtaining an improved transfer function under the traditional Nyquist criterion, and is not used for stability analysis directly yet. The describing function and its deducing method for the nonlinear switching link in power converters are still not mature.

In this paper, a PWM boost converter is taken as an example, and the describing function of the switching process in DC-DC converters is firstly deduced. Its traditional linear model and the nonlinear model based on describing function method are established, respectively. Finally, the simulation and experimental results are given to validate the correctness and effectiveness of nonlinear stability analysis based on describing function.

II. MODELING AND STABILITY CRITERION FOR THE DC-DC CONVERTERS

It is well known that boost converter is a basic topology of DC-DC converters, which has gained wide application in photovoltaic inverters, wind power generations in recent years. In this paper, a boost converter is taken as an example for modeling and stability analysis.

The boost converter with its closed-loop control is shown in Fig. 1(a), where, its control is a voltage closed-loop including a PI controller.

A. THE LINEAR MODEL OF THE BOOST CONVERTER AND ITS STABILITY CRITERION

The small signal modeling method is adopted in the boost converter for linear modeling. The small signal diagram of the boost converter [30] is shown in Fig. 1(b), which can be further simplified as shown in Fig. 1(c) [31]. The transfer function of each link in Fig. 1 can be expressed in (1).

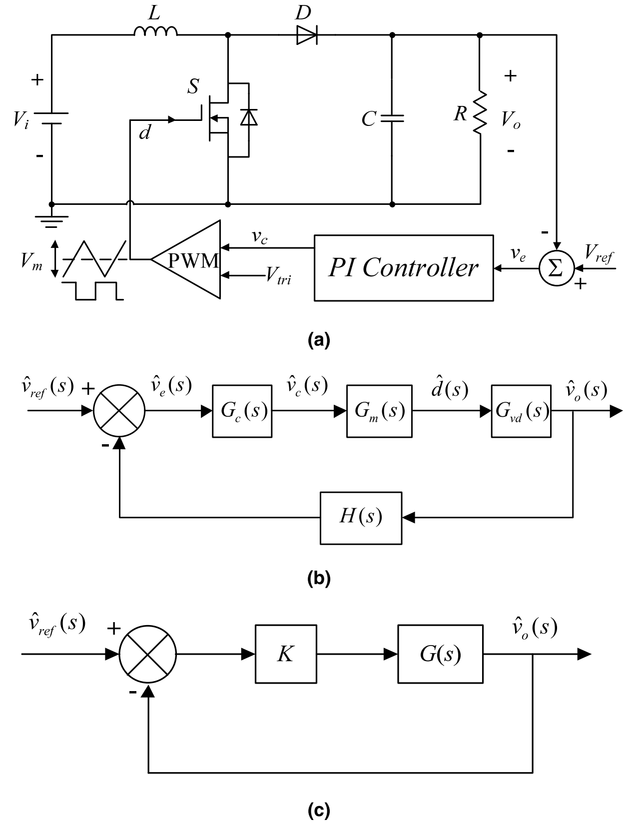

FIGURE 1. The structure diagram of boost converter. (a) The closed-loop circuit of boost converter with PI controller. (b) The block diagram of the boost converter. (c) The simplified diagram of the boost converter.

$$\begin{cases} K = G_m(s) = \dfrac{1}{V_m} \\ G(s) = G_c(s)G_{vd}(s) \\ \quad = [\dfrac{K_p(1+T_i s)}{T_i s}][\dfrac{V_i}{D'^2}\dfrac{1-s\frac{L}{D'^2R}}{1+s\frac{L}{D'^2R}+s^2\frac{LC}{D'^2}}] \\ H(s) = 1. \end{cases} \tag{1}$$

In Fig. 1(c), K represents the switching process of S in the boost converter, which is a nonlinear link. But in the linear model, the switching process is averaged and is expressed by $\frac{1}{V_m}$.

In traditional Nyquist stability analysis method, when the transfer functions of a system are obtained, the Nyquist plot can be drawn out to determine the stability of the system [32]. For the boost converter system shown in Fig. 1(c), its closed loop transfer function can be expressed as (2).

$$\frac{\hat{v}_o(s)}{\hat{v}_{ref}(s)} = \frac{KG(s)}{1+KG(s)}. \tag{2}$$

The characteristic equation of (2) is $1+KG(s)=0$, or

$$G(s) = -\frac{1}{K} + j0. \tag{3}$$

Therefore, the stability of the boost converter can be judged by the position relationship between the Nyquist plot of $G(s)$ and the point of $(-\frac{1}{K}, j0)$.

B. THE NONLINEAR MODEL BASED ON DESCRIBING FUNCTION OF THE BOOST CONVERTER AND ITS STABILITY CRITERION

The basic idea of the describing function (DF) method is to replace each nonlinear link with a describing function, which is a ratio of the first harmonic of the nonlinear link output and a sinusoidal signal input [33]. According to the obtained describing function, the fundamental frequency characteristic of the nonlinear link can be derived.

Giving a sinusoidal input signal Asin to the nonlinear link, the Fourier transform of the nonlinear link output y can be expressed as:

$$\begin{aligned} y(t) &= A_0 + \sum_{n=1}^{\infty} (A_n \cos n\omega t + B_n \sin n\omega t) \\ &= A_0 + \sum_{n=1}^{\infty} Y_n \sin(n\omega t + \varphi_n). \end{aligned} \tag{4}$$

When the $A_0 = 0$ and $n > 1$, Y_n are usually very small, the sinusoidal response of the nonlinear element can be approximately replaced by the first harmonic:

$$y(t) = A_1 \cos \omega t + B_1 \sin \omega t = Y_1 \sin(\omega t + \varphi_1). \tag{5}$$

According to [21], the describing function can be defined as the plural ratio of the first harmonic of nonlinear link output and the sinusoidal input signal:

$$N(A) = |N(A)|\, e^{j\angle N(A)} = \frac{Y_1}{A} e^{j\varphi_1} = \frac{B_1 + jA_1}{A}, \tag{6}$$

where, A is the amplitude of the sinusoidal input signal.

Fig. 1(c) shows the linear model of the boost converter. To get the nonlinear model based on DF method, $N(A)$, the describing function of the switching process, is used to replace the K in Fig. 1(c), and the nonlinear model is shown in Fig. 2.

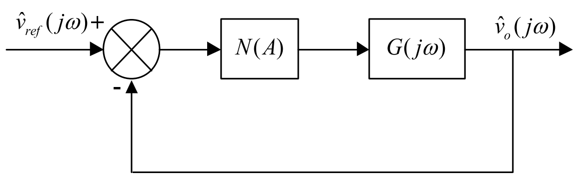

FIGURE 2. The nonlinear model of the boost converter.

Similar to the linear system, the closed loop transfer function of the model can be derived as (7).

$$\frac{\hat{v}_o(j\omega)}{\hat{v}_{ref}(j\omega)} = \frac{N(A)G(j\omega)}{1 + N(A)G(j\omega)}. \tag{7}$$

According to (7), its characteristic equation can be expressed as $1 + N(A)G(j\omega) = 0$, or:

$$G(j\omega) = -\frac{1}{N(A)}. \tag{8}$$

Then, the Nyquist plot of $G(j\omega)$ and $-\frac{1}{N(A)}$ can be drawn in complex plane. So, the stability of the converter can be determined by observing the positional relationship of these two curves. As shown in Fig. 3, if the $G(j\omega)$ curve separates from the $-\frac{1}{N(A)}$ curve, the system is stable; if the $G(j\omega)$ curve surrounds the $-\frac{1}{N(A)}$ curve, the system is unstable; and if the two curves intersect, the system is critical stable [31], [34], [35].

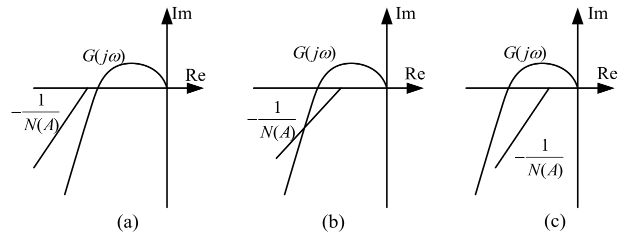

FIGURE 3. Stability analysis for describing function method.

Comparing the linear model with the nonlinear model based on the describing function method, it can be found that the transfer function of the linear links are the same, namely, $G(j\omega) = G(s)$. Therefore, $G(j\omega)$, the point $(-\frac{1}{K}, j0)$ and the $-\frac{1}{N(A)}$ can be plotted in the same complex plane. By observing the positional relationship of $G(j\omega)$, $(-\frac{1}{K}, j0)$ and the $-\frac{1}{N(A)}$, the stability can be determined by the traditional linear method and describing function method, respectively.

III. THE DESCRIBING FUNCTION DERIVATION OF THE SWITCHING PROCESS

In the linear model of boost converter, the switching process is averaged. But because the switching process is nonlinear in essence, the averaged model cannot fully express the characteristics of the switching process. Therefore, a nonlinear model based on describing function is constructed in this paper.

According to the definition of the describing function, assuming that the input of the switching link is sinusoidal signal: $v_{in} = A\cos y$, where, $y = \omega_0 t$, as shown in Fig. 4. In addition, the peak-to-peak value of the triangle carrier used in PWM is V_m and the frequency of the triangular carrier is ω_c. Finally, the output waveform of the PWM link is a square wave with amplitudes of $\pm V_d$, which can be further expanded to a Fourier series: $v_p(t) = \frac{a_0}{2} + \sum_{m=1}^{\infty} (a_m \cos mx + b_m \sin mx)$, where, $x = \omega_c t$, as shown in Fig. 4.

There is no direct component in $v_p(t)$, so $a_0 = 0$. After calculation, $v_p(t)$ can be expressed as [36]:

$$\begin{aligned} v_p(t) = &\frac{2V_d A \cos y}{V_m} \\ &+ \frac{4V_d}{\pi} \sum_{m=1}^{\infty} \frac{1}{m} J_0\left(m\pi \frac{A}{V_m}\right) \sin m\frac{\pi}{2} \cos mx \\ &+ \frac{4V_d}{\pi} \sum_{m=1}^{\infty} \sum_{n=1}^{\infty} \frac{1}{m} J_n\left(m\pi \frac{A}{V_m}\right) \sin\left[(m+n)\frac{\pi}{2}\right] \\ &\cdot [\cos(mx + ny) + \cos(mx - ny)]\,. \end{aligned} \tag{9}$$

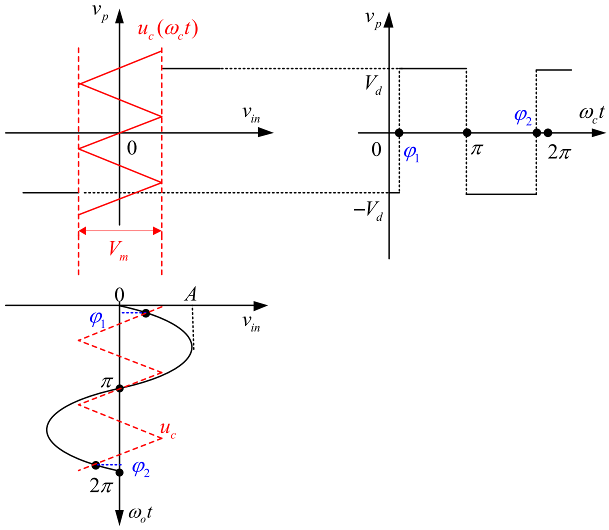

FIGURE 4. Triangular carrier compared with low frequency signal to generate the PWM waveforms.

Because carrier frequency ω_c is normally much greater than the modulation waveform frequency ω_0, let $x = \frac{\omega_c y}{\omega_0} = ky$, and $k \gg 1$. After substitution, the (9) can be expressed as (10):

$$v_p(t) = \frac{2V_d A \cos y}{V_m} \ldots\ldots item1$$
$$+ \frac{4V_d}{\pi} \sum_{m=1}^{\infty} \begin{bmatrix} \frac{1}{m} J_0 \left(m\pi \frac{A}{V_m}\right) \\ \cdot \sin m\frac{\pi}{2} \cos(kmy) \end{bmatrix} \ldots item2$$
$$+ \frac{4V_d}{\pi} \sum_{m=1}^{\infty} \sum_{n=1}^{\infty} \begin{bmatrix} \frac{1}{m} J_n \left(m\pi \frac{A}{V_m}\right) \\ \cdot \sin \left([m+n]\frac{\pi}{2}\right) \\ \cdot \cos(kmy + ny) \end{bmatrix} \ldots item3$$
$$+ \frac{4V_d}{\pi} \sum_{m=1}^{\infty} \sum_{n=1}^{\infty} \begin{bmatrix} \frac{1}{m} J_n \left(m\pi \frac{A}{V_m}\right) \\ \cdot \sin \left([m+n]\frac{\pi}{2}\right) \\ \cdot \cos(kmy - ny) \end{bmatrix} \ldots item4. \quad (10)$$

In order to get the fundamental components in (10), *item*1-*item*4 should be considered separately. For *item*1, it is a fundamental component obviously. For *item*2 and *item*3, no fundamental component is included in these two items because it is impossible to make $\cos kmy = \cos y$ and $\cos(kmy + ny) = \cos y$, since m and n are positive integers and $k \gg 1$. For *item*4, it has fundamental component when $\cos(kmy-ny) = \cos y$, that is when $km-n = 1$. Then, the fundamental components of the output $v_p(t)$ can be expressed as (11) by substituting $km - n = 1$ into *item*4 of (10).

$$v_p(t) = \frac{2V_d A \cos y}{V_m} + \frac{4V_d}{\pi} \sum_{m=1}^{\infty} \left\{ \begin{array}{l} \frac{1}{m} J_{km-1} \left(m\pi \frac{A}{V_m}\right) \\ \cdot \sin \left([(k+1)m - 1]\frac{\pi}{2}\right) \\ \cdot \cos y \end{array} \right\}. \quad (11)$$

According to the practical application, V_d can be set to be 0.5. Then, the describing function of the nonlinear link is the ratio between $v_p(t)$ and the input signal $A \cos y$, namely, $N(A)$.

$$N(A) = \frac{v_p(t)}{v_{in}} = \frac{1}{V_m} + \frac{2}{\pi A} \sum_{m=1}^{\infty} \left\{ \begin{array}{l} \frac{1}{m} J_{km-1} \left(m\pi \frac{A}{V_m}\right) \cdot \\ \sin \left([(k+1)m - 1]\frac{\pi}{2}\right) \end{array} \right\}. \quad (12)$$

In (12), A is the amplitude of the modulation waveform, $J_{km-1}\left(m\pi \frac{A}{V_m}\right)$ is the first kind Bessel function.

When the expression of $N(A)$ is obtained, as given in (12), the following question is how to determine the parameters of $N(A)$ in practice, since $N(A)$ includes k, A and an infinite series. With these parameters, the output range of $N(A)$ will thereby be determined and drawn up.

IV. PARAMETER DETERMINATION FOR THE DESCRIBING FUNCTION OF THE SWITCHING PROCESS

For the $N(A)$, the upper limit of m should be infinite, k ranges from k_{min} to infinite and A ranges from 0 to infinite.

To obtain the effective and practical function describing function of the switching process, firstly, the limit of the obtained describing function is proved and calculated in this paper.

A. DETERMINATION FOR THE RANGE OF m

1) THE PROOF OF CONVERGENCE FOR THE DESCRIBING FUNCTION

For any determined k and A, the $\frac{1}{V_m}$ and $\frac{2}{\pi A}$ do not affect the convergence of $N(A)$, so the convergence of series $N_m = \sum_{m=1}^{\infty} \frac{1}{m} J_{km-1}\left(m\pi \frac{A}{V_m}\right) \sin\left([(k+1)m - 1]\frac{\pi}{2}\right)$ is taken into consideration.

Assuming that N'_m is the absolute value of N_m:

$$N'_m = |N_m| = \left| \sum_{m=1}^{\infty} \begin{array}{l} \frac{1}{m} J_{km-1} \left(m\pi \frac{A}{V_m}\right) \\ \cdot \sin \left([(k+1)m - 1]\frac{\pi}{2}\right) \end{array} \right|. \quad (13)$$

According to the theory of Bessel functions [37], [38], it can be concluded that:

$$N'_m = \left| \sum_{m=1}^{\infty} \begin{array}{l} \frac{1}{m} J_{km-1} \left(m\pi \frac{A}{V_m}\right) \\ \cdot \sin \left([(k+1)m - 1]\frac{\pi}{2}\right) \end{array} \right| < \sum_{m=1}^{\infty} \frac{1}{m} [J_{km-1}(x)]_{\max} = N''_m, \quad (14)$$

where, N''_m and N'_m are both positive series.

For the maximum value of Bessel's function, there is $[J_\alpha(x)]_{\max} < \sqrt[3]{\frac{1}{\alpha}}$, as shown in Fig. 5.

Thus, $N''_m < \sum_{m=1}^{\infty} \frac{1}{m} \sqrt[3]{\frac{1}{km-1}}$, further, $N''_m < \sum_{m=1}^{\infty} \frac{1}{m} \sqrt[3]{\frac{1}{(k-1)m}} = \sum_{m=1}^{\infty} \frac{1}{(k-1)^{\frac{1}{3}}} \frac{1}{m^{\frac{4}{3}}} = N'''_m$. Obviously, N'''_m is a p-series, as $k \gg 1$, and $\frac{4}{3} > 1$, so N'''_m is convergent.

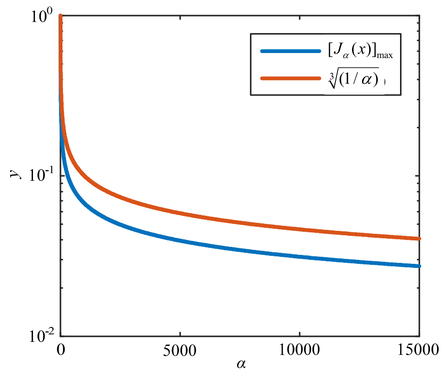

FIGURE 5. The changing curves of $[J_\alpha(x)]_{\max}$ and $\sqrt[3]{\frac{1}{\alpha}}$ with the increase of α.

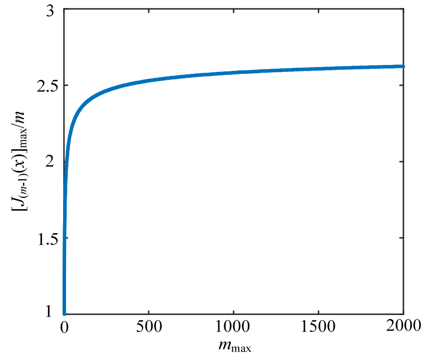

FIGURE 6. The changing curves of N''_m with the increase of the upper limit of m.

Theorem 1: If both $\sum_{n=1}^{\infty} u_n$ and $\sum_{n=1}^{\infty} v_n$ are series with positive terms, and $u_n \leq v_n$ $(n = 1, 2, 3, \ldots)$. If the $\sum_{n=1}^{\infty} v_n$ is convergent, then the $\sum_{n=1}^{\infty} u_n$ is convergent [39].

According to Theorem 1, N'''_m is convergent, so N''_m and N'_m are convergent.

Theorem 2: If the series $\sum_{n=1}^{\infty} u_n$ is absolute convergence, the series $\sum_{n=1}^{\infty} v_n$ must be convergent [39].

According to Theorem 2, when N'_m is convergent, N_m is also convergent.

2) COMPARISON OF RATE OF CONVERGENCE BETWEEN N''_m AND N_m

Because sinusoidal function does not affect the rate of convergence, so the sinusoidal component is neglected for the comparison:

$$\lim_{m\to\infty} \frac{N_m}{N''_m} \xrightarrow[\text{convergence}]{\text{rate of}} \lim_{m\to\infty} \frac{\frac{1}{m}J_{km-1}(x)}{\frac{1}{m}J_{km-1}(x)_{\max}} = \lim_{m\to\infty} \frac{J_{km-1}(x)}{J_{km-1}(x)_{\max}} = r. \quad (15)$$

Since $J_{km-1}(x) \leq J_{km-1}(x)_{\max}$ always stands up, so $r \leq 1$. It means that the rate of convergence of N_m is faster or same with N''_m. So, the upper limit of m can be determined by N''_m.

3) DETERMINATION OF THE UPPER LIMIT OF m

Assuming that $k = 1$, the changing curve of N''_m with the increase of the upper limit of m is shown in Fig. 6. The inflection point of the changing curve of N''_m is about 800, so the upper limit of m is taken as 800.

So, the range of m is 1-800.

B. DETERMINATION FOR THE RANGE OF k

In this paper, $k = \frac{\omega_c}{\omega_0}$, which means the ratio between the carrier frequency and the frequency of the input sinusoidal signal. In practice, k is always a big number, therefore, it can be thought a number larger than 10, that is $k_{min} = 10$.

Constraint relation of k and A: For a certain frequency, when A increases to A_{max}, the switching pulse square waveforms will be the same for all the $A > A_{max}$, as shown in Fig. 7. So, A should be less than A_{max}.

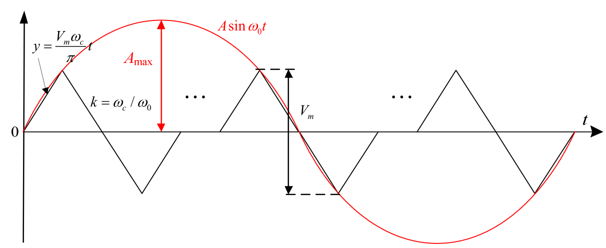

FIGURE 7. Triangular carrier wave and low frequency signal input.

From that $A_{\max} \sin \omega_0 t = \frac{V_m \omega_c}{\pi} t$, $t = \frac{\pi}{2\omega_c}$, the constraint relation of k and A can be expressed as:

$$A \leq \frac{V_m}{2\sin(\pi/2k)}. \quad (16)$$

To simplify the calculation, V_m is set as 1 in this paper. Therefore, for all $A \leq \frac{1}{2\sin(\pi/2k)}$, there is $km - 1 > m\pi \frac{A}{V_m}$, which means $\frac{2}{m\pi A} J_{km-1}\left(m\pi \frac{A}{V_m}\right) > 0$.

1) DETERMINATION FOR THE UPPER LIMIT OF k

Because $\frac{2}{m\pi A} J_{km-1}\left(m\pi \frac{A}{V_m}\right) > 0$ and $V_m = 1$, there is:

$$N(A) = \frac{1}{V_m} + \sum_{m=1}^{\infty} \left\{ \begin{array}{l} \frac{2}{m\pi A} J_{km-1}\left(m\pi \frac{A}{V_m}\right) \\ \cdot \sin\left([(k+1)m - 1]\frac{\pi}{2}\right) \end{array} \right\} < \frac{1}{V_m} + \sum_{m=1}^{\infty} \frac{2}{m\pi A} J_{km-1}\left(m\pi \frac{A}{V_m}\right)$$

Let $x = m\pi A$, there is

$$N(A) < 1 + \sum_{m=1}^{\infty} \frac{2}{x} J_{km-1}(x) < 1 + \sum_{m=1}^{\infty} \left[\frac{2J_{km-1}(x)}{x}\right]_{\max}. \quad (17)$$

Since $y(k)=\sum_{m=1}^{\infty}\left[\frac{2J_{km-1}(x)}{x}\right]_{\max}$ is a monotone decreasing function, the range of $N(A)$ can be approximately determined by $1+y(k)$ and $1-y(k)$, as shown in Fig. 8.

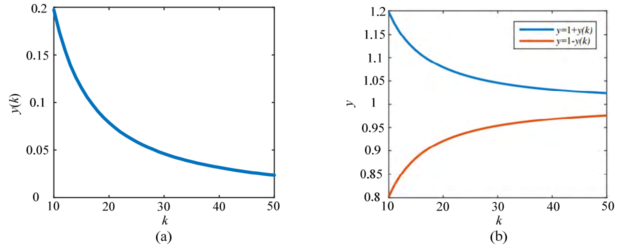

FIGURE 8. The function curves which are used to determine the range of $N(A)$. (a) The $y(k)$ function. (b) $1+y(k)$ and $1-y(k)$.

When k is taken from 10 to 42, the actual region of $N(A)$ is shown in Fig. 9. When $k=42$, the $N(A)$ curve intersects with $1+y(k)$ and $1-y(k)$, which means the region of $N(A)$ for all the $k>42$ will be included in the region of $N(A)$ for $10\le k\le 42$. So $k_{max}=42$. So, the range of k is 10-42.

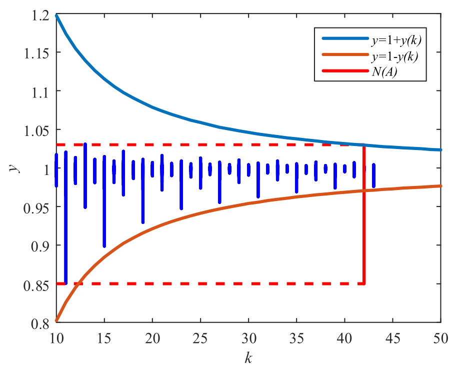

FIGURE 9. The curves of $1\pm y(k)$ and $N(A)$ with the changing of k.

C. DETERMINATION FOR THE RANGE OF A

As mentioned above: $A\le\frac{V_m}{2\sin(\pi/2k)}$. Taken $V_m=1$ and $k=42$, the maximum value of A can be determined: $A_{max}=14$.

For the lower limit of A, it can be determined by the following proof.

$$\lim_{A\to0}N(A)=\frac{1}{V_m}+\lim_{A\to0}\left\{\sum_{m=1}^{\infty}\left[\begin{array}{l}\frac{2}{m\pi A}\cdot J_{km-1}(m\pi\frac{A}{V_m})\\ \cdot\sin\left([(k+1)m-1]\cdot\frac{\pi}{2}\right)\end{array}\right]\right\}. \tag{18}$$

In (18), the first kind Bessel function $J_{km-1}(m\pi\frac{A}{V_m})$ can be expanded to Taylor series, as shown in (19),

$$J_{km-1}(m\pi\frac{A}{V_m})=\sum_{a=0}^{\infty}\left(\begin{array}{l}\frac{(-1)^a}{a!\Gamma(a+km)}\\ \cdot(\frac{m\pi A}{2V_m})^{2a+km-1}\end{array}\right). \tag{19}$$

Then,

$$\begin{aligned}&\lim_{A\to0}\left\{\sum_{m=1}^{\infty}\left[\begin{array}{l}\frac{2}{m\pi A}\cdot J_{km-1}(m\pi\frac{A}{V_m})\\ \cdot\sin\left([(k+1)m-1]\cdot\frac{\pi}{2}\right)\end{array}\right]\right\}\\ &=\lim_{A\to0}\left\{\sum_{m=1}^{\infty}\left[\begin{array}{l}\frac{2}{m\pi A}\\ \cdot\sum_{a=0}^{\infty}\left(\begin{array}{l}\frac{(-1)^a}{a!\Gamma(a+km)}\\ \cdot(\frac{m\pi A}{2V_m})^{2a+km-1}\end{array}\right)\\ \cdot\sin\left([(k+1)m-1]\cdot\frac{\pi}{2}\right)\end{array}\right]\right\}\\ &=\lim_{A\to0}\left\{\sum_{m=1}^{\infty}\left[\begin{array}{l}2\cdot\sum_{a=0}^{\infty}\left(\begin{array}{l}\frac{(-1)^a}{a!\Gamma(a+km)}\\ \cdot(\frac{1}{2V_m})^{2a+km-1}\\ \cdot(m\pi A)^{2a+km-2}\end{array}\right)\\ \cdot\sin\left([(k+1)m-1]\cdot\frac{\pi}{2}\right)\end{array}\right]\right\}.\end{aligned} \tag{20}$$

In (20),

$$\begin{aligned}&\lim_{A\to0}\left(2\cdot\sum_{a=0}^{\infty}\left(\begin{array}{l}\frac{(-1)^a}{a!\Gamma(a+km)}\\ \cdot(\frac{1}{2V_m})^{2a+km-1}\\ \cdot(m\pi A)^{2a+km-2}\end{array}\right)\right)\\ &=\lim_{A\to0}\left(\begin{array}{l}\frac{2\cdot(-1)^a}{a!\Gamma(a+km)}\\ \cdot(\frac{1}{2V_m})^{2a+km-1}\\ \cdot(m\pi A)^{2a+km-2}\end{array}\right)\Bigg|_{a=0}\\ &\quad+\lim_{A\to0}\left(2\cdot\sum_{a=1}^{\infty}\left(\begin{array}{l}\frac{(-1)^a}{a!\Gamma(a+km)}\\ \cdot(\frac{1}{2V_m})^{2a+km-1}\\ \cdot(m\pi A)^{2a+km-2}\end{array}\right)\right).\end{aligned} \tag{21}$$

As mentioned above: the range of m is 1-800, and the range of k is 10-42, so $km\ge 10$, which means $\Gamma(km)>0$ and $\Gamma(a+km)>0$, then (21) can be calculated as

$$\begin{aligned}&\lim_{A\to0}\left(2\cdot\sum_{a=0}^{\infty}\left(\begin{array}{l}\frac{(-1)^a}{a!\Gamma(a+km)}\\ \cdot(\frac{1}{2V_m})^{2a+km-1}\\ \cdot(m\pi A)^{2a+km-2}\end{array}\right)\right)\\ &=\left(\begin{array}{l}\frac{2\cdot(-1)^0}{0!\Gamma(0+km)}\\ \cdot(\frac{1}{2V_m})^{2\times0+km-1}\\ \cdot(m\pi\cdot0)^{2\times0+km-2}\end{array}\right)\\ &\quad+\left(2\cdot\sum_{a=1}^{\infty}\left(\begin{array}{l}\frac{(-1)^a}{a!\Gamma(a+km)}\\ \cdot(\frac{1}{2V_m})^{2a+km-1}\\ \cdot(m\pi\cdot0)^{2a+km-2}\end{array}\right)\right)\\ &=0.\end{aligned} \tag{22}$$

According to (18)-(22), when $A=0$, $N(A)$ can be expressed as:

$$N(A)=\frac{1}{V_m}. \tag{23}$$

Therefore, the range of A is 0-14.

According to the above mathematical analysis, the regions of the parameters in $N(A)$ can be determined as follows: the upper limit of m is determined as 800, the range of k is determined as 10-42, and A is determined as 0-14.

Fig. 10 gives the plot of $-\frac{1}{N(A)}$ with different A and k, in which *The projection of the 3D plot on z axis* actually is the curve of $-\frac{1}{N(A)}$.

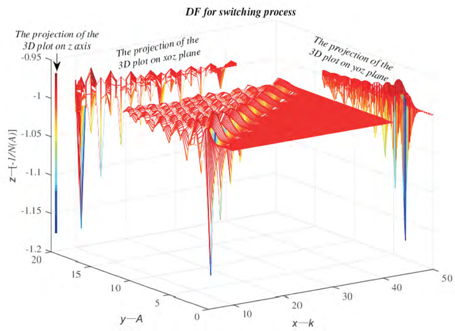

FIGURE 10. The plot of $-\frac{1}{N(A)}$ with different A and k.

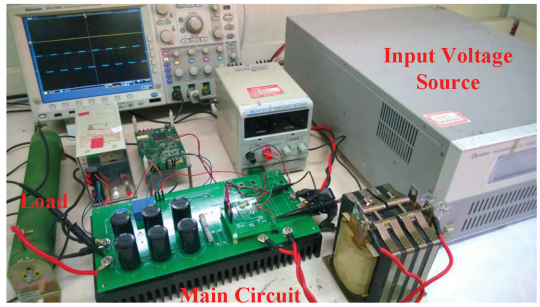

FIGURE 11. The experiment platform of the boost converter.

Therefore, the describing function of the PWM switching process can be expressed as:

$$N(A) = \frac{1}{V_m} + \frac{2}{\pi A} \sum_{m=1}^{800} \left(\begin{array}{l} \frac{1}{m} J_{km-1}\left(m\pi \frac{A}{V_m}\right) \\ \cdot \sin\left([(k+1)m - 1]\frac{\pi}{2}\right) \end{array} \right). \quad (24)$$

It should be noticed that (24) not only can be used for the boost converter in this paper, but also can be used for other PWM DC-DC converters.

V. SIMULATION AND EXPERIMENTAL VERIFICATION

In this paper, MATLAB is used to draw the Nyquist curve, and PSIM is used to simulate the boost circuit. Finally, the results are validated by experiment. The simulation and experimental parameters are shown in Table 1, and the types and parameters of experimental instruments are shown in Table 2. The experiment platform is shown in Fig. 11. Under the parameters, the stability of the system can be determined by determining the positional relationship between the Nyquist curve of $G(s)$ and $-\frac{1}{N(A)}$.

TABLE 1. Simulation and experimental parameters.

Input Voltage(V)	Output Voltage(V)	Switching Frequency (Hz)	Capacitance (μF)
12	24	100k	280
Inductance (mH)	Load Resistance (Ω)	PWM Amplitude (V)	Sampling Ratio
0.4	6	1	1

TABLE 2. Types and parameters of experimental instruments.

Instruments	Types	Parameters
DC power supply	Chroma 62050P	0-600V
Auxiliary power supply	WD-990	5V/±12V/±15V
Oscilloscope	Tektronix DPO4054B	500MHz
Voltage probe	Tektronix P220	200MHz/600V
DSP control board	TMS320F28335	

Since the proposed describing function method focuses on the nonlinear PWM link, and the models for the other linear links are all obtained by the traditional linear modeling, the stability analysis based on describing function method will be compared with the traditional Nyquist method.

In order to compare the result of the traditional Nyquist method and the describing function method in the stability analysis of the boost converter, the PI parameters K_p and T_i in $G_c(s)$ are modified continuously to make the intersection point of the Nyquist curve $G(s)$ and real axis move in the negative direction. And the system state changes from stable mode to unstable mode, as shown in Fig. 12.

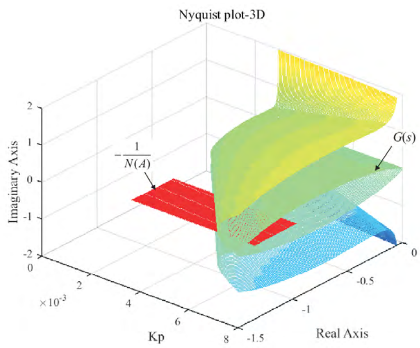

FIGURE 12. The 3 dimension Nyquist plot with the changing K_p.

Four typical cases are listed in Table 3.

TABLE 3. Comparisons of the results obtained by different methods.

Methods	Case I	Case II	Case III	Case IV
Traditional linear method	stable	stable	unstable	unstable
Describing function method	stable	critical stable	critical stable	unstable
Simulation experiment results	stable	critical stable	critical stable	unstable

Case I (K_p = 0.003, T_i = 0.0005): Fig. 13(a) shows the Nyquist curve of $G(s)$ and $-\frac{1}{N(A)}$, Fig. 13(b) shows the simulation waveform and Fig. 13(c) shows the experimental waveform of the output voltage.

Under the Case I, the Nyquist curve of $G(s)$ does not surround the point $(-1, j0)$ and the $-\frac{1}{N(A)}$ curve. Due to

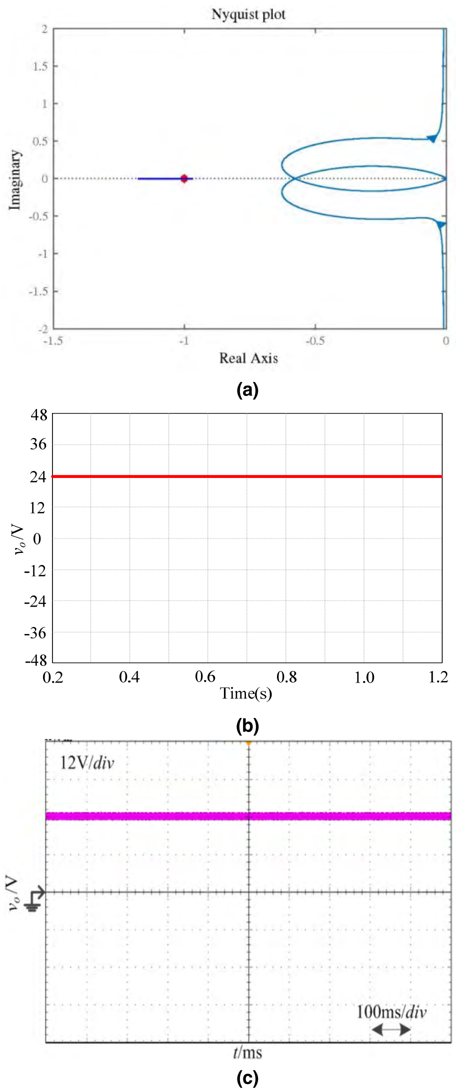

FIGURE 13. **The Nyquist plot and waveforms under Case I. (a) The Nyquist plot in Case I. (b) The simulation waveform of the output voltage. (c) The experiment waveform of the output voltage.**

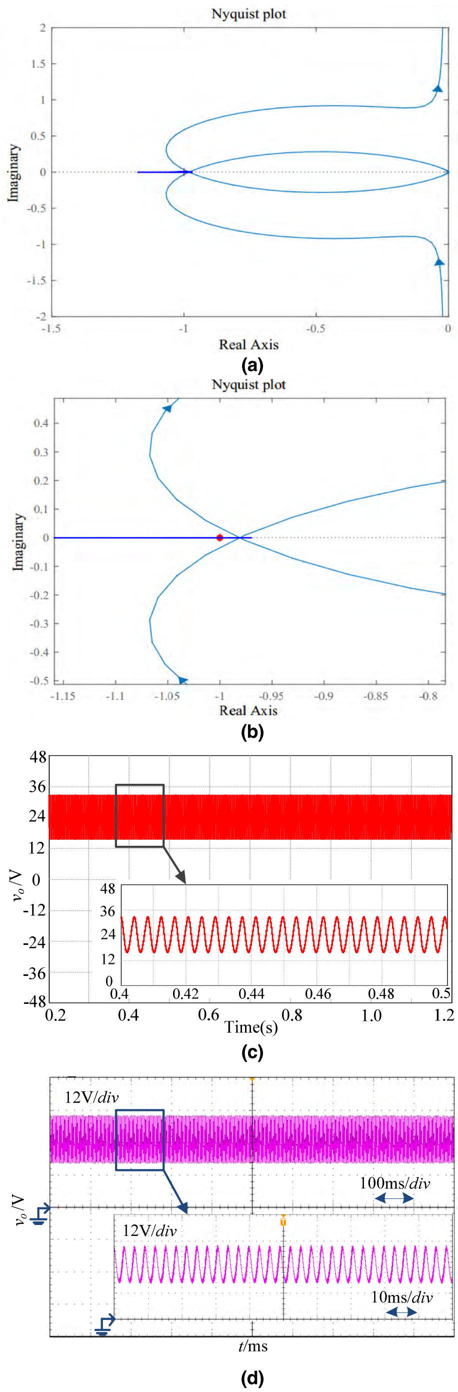

FIGURE 14. **The Nyquist plot and waveforms under Case II. (a) The Nyquist plot in Case II. (b) The enlarged drawing of the crossing point. (c) The simulation waveform of the output voltage. (d) The experiment waveform of the output voltage.**

the traditional Nyquist stability criterion and the method of describing function criterion, the system is stable.

Case II ($K_p = 0.0051$, $T_i = 0.0005$): Fig. 14(a) shows the Nyquist curve of $G(s)$ and $-\frac{1}{N(A)}$, Fig. 14(b) shows the enlarged drawing of the crossing point. Fig. 14(c) shows the simulation waveform and Fig. 14(d) shows the experimental waveform. And the bottom right corners show the enlarged drawing.

Under the Case II, the Nyquist curve of $G(s)$ does not surround the point $(-1, j0)$ but intersects the $-\frac{1}{N(A)}$ curve. The system is stable with the traditional Nyquist stability criterion, but critical stable with the describing function criterion.

Case III ($K_p = 0.0055$, $T_i = 0.0005$): Fig. 15(a) shows the Nyquist curve of $G(s)$ and $-\frac{1}{N(A)}$. Fig. 15(b) shows the simulation waveform and Fig. 15(c) shows the experimental waveform. And the bottom right corners show the enlarged drawing.

Under the Case III, the Nyquist curve of $G(s)$ surrounds the point $(-1, j0)$ and intersects the $-\frac{1}{N(A)}$ curve. The system is unstable with the traditional Nyquist stability criterion, but critical stable with the describing function criterion.

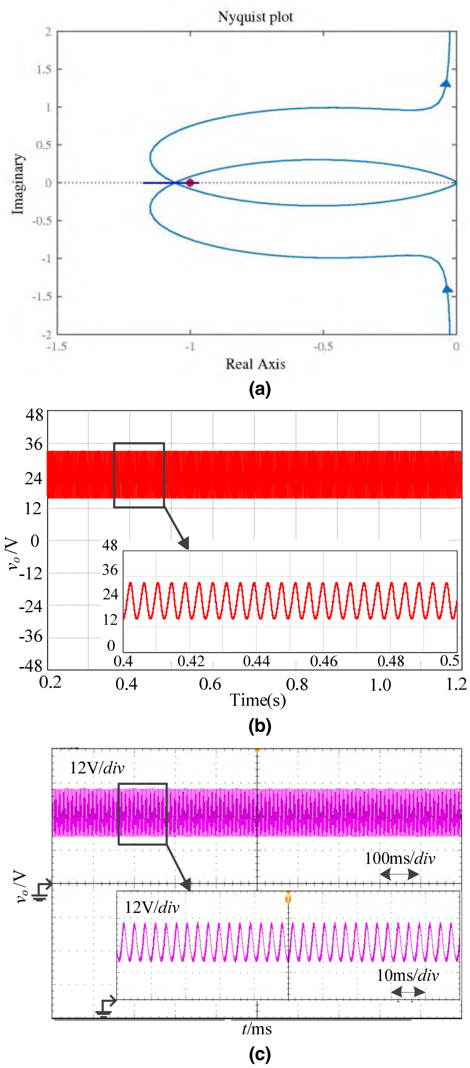

FIGURE 15. The Nyquist plot and waveforms under Case III. (a) The Nyquist plot in Case III. (b) The simulation waveform of the output voltage. (c) The experiment waveform of the output voltage.

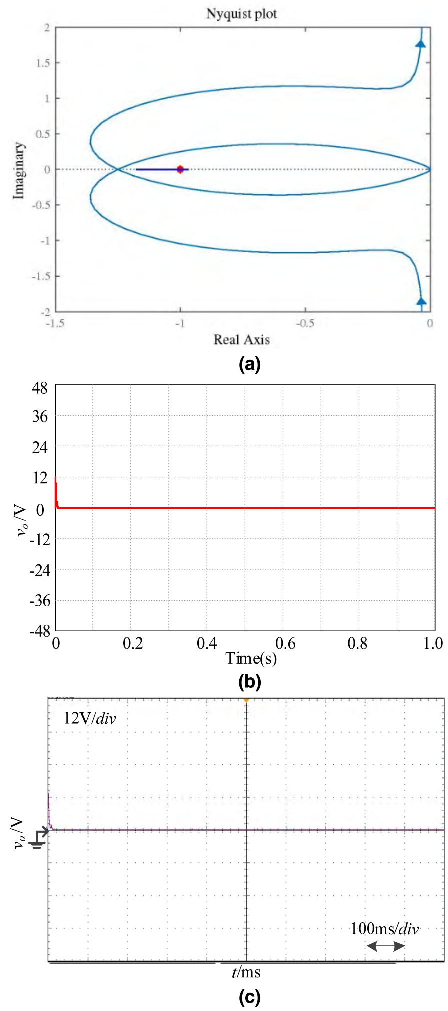

FIGURE 16. The Nyquist plot and waveforms under Case IV. (a) The Nyquist plot in Case IV. (b) The simulation waveform of the output voltage. (c) The experiment waveform of the output voltage.

Case IV ($K_p = 0.0065$, $T_i = 0.0005$): Fig. 16(a) shows the Nyquist curve of $G(s)$ and $-\frac{1}{N(A)}$. Fig. 16(b) shows the simulation waveform and Fig. 16(c) shows the experimental waveform.

Under the Case IV, the Nyquist curve of $G(s)$ surrounds both the point $(-1, j0)$ and the $-\frac{1}{N(A)}$ curve. The system is unstable due to the two stability criterion.

In summary, in Case I and IV, the stability analysis results are same with both the traditional Nyquist analysis and the describing function method, the simulation and experimental results demonstrate the validity of the analysis. In Case II and III, according to traditional Nyquist analysis, the system is in stable state and unstable state, respectively; but according to the describing function method, the system is both in critical stable state. From the simulation and experimental waveforms, in the two cases, the output voltage has low frequency oscillation phenomena, but the voltage waveform is not divergent yet, which confirms that the analysis of the describing function method is more accurate. Case II and III are set in the transition interval from stable region to unstable region, and the stability analysis based on describing function method can determine the transition interval while traditional Nyquist stability analysis cannot determine it.

VI. TRANSITION INTERVAL DETERMINATION

According to the analysis in section V, it is obvious that finding the transition interval from stable region to unstable region, namely, the critical stable range, is very important. Because this critical stable range can be regarded as the stability margins in the traditional linear stability analysis.

With the obtained describing function $N(A)$ of the switching process for the boost converter, it can be found that $-\frac{1}{N(A)}$ is a line on the real axis, and the range of $-\frac{1}{N(A)}$ can be obtained easily, as shown in Fig. 17. According to calculation

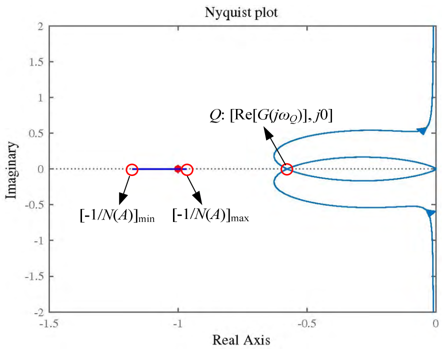

FIGURE 17. The Nyquist plot of the boost converter.

and Fig. 10, $\left[-\frac{1}{N(A)}\right]_{\min} = -1.174$ and $\left[-\frac{1}{N(A)}\right]_{\max} = -0.97$ in this paper.

Further, according to the stability criterion in Fig. 3, if $G(j\omega)$ and $-\frac{1}{N(A)}$ intersect, the boost converter is critical stable. Therefore, the point Q, the intersection point between the curve of $G(j\omega)$ and real axis, should be determined. Obviously, $Im[G(j\omega Q)] = 0$, here, ω_Q means the frequency at the point Q. According to $Im[G(j\omega Q)] = 0$, the frequency ω_Q can be calculated, as given in (25).

$$\omega_Q = \sqrt{\frac{b + \sqrt{b^2 + 4a}}{2a}}. \qquad (25)$$

where, $a = \frac{L^2CT_i}{D'^4R}$, $b = \frac{LT_i}{D'^2R} - \frac{LC}{D'^2} + \frac{L}{D'^2R}(T_i - \frac{L}{D'^2R})$.

Then, substituting the obtained ω_Q into $G(j\omega)$ in (1), the real part of the point Q can be expressed by a function of control parameters K_p and T_i, as given in (26).

$$Re[G(j\omega_Q)] = \frac{K_pV_i}{D'^2T_i} \cdot [\frac{-\frac{L}{D'^2R}(1 + \omega_Q{}^2\frac{LT_i}{D'^2R}) + (T_i - \frac{L}{D'^2R})(1 - \omega_Q{}^2\frac{LT_i}{D'^2R})}{\omega_Q{}^2(\frac{L}{D'^2R})^2 + 1 - 2\omega_Q{}^2\frac{LC}{D'^2} + \omega_Q{}^4(\frac{LC}{D'^2})^2}]. \qquad (26)$$

According to Fig. 3 and Fig. 17, when $\left[-\frac{1}{N(A)}\right]_{\min} \leq Re[G(j\omega_Q)] \leq \left[-\frac{1}{N(A)}\right]_{\max}$, this boost converter will be under critical stable mode. Therefore, the ranges of K_p and T_i in critical stable mode, i.e. in the transition interval, can be calculated.

In this paper, with $T_i = 0.0005$, when $0.0050 \leq K_p \leq 0.0061$, this boost converter will be under critical stable mode; with $K_p = 0.003$, when $0.000238 \leq T_i \leq 0.000289$, this boost converter will be under critical stable mode. For other situations, the control parameter range can be determined according the above mentioned method.

VII. FURTHER VERIFICATION

To further verify the accuracy and correctness of the proposed stability analysis based on describing function method, the bifurcation diagram of the output voltage is also plotted by iterative equations of the boost converter.

Assuming that $X = [\, v_C \; i_L \,]^T$, the state equations of the boost converter can be expressed as (27):

$$\begin{cases} \dot{X} = A_1X \\ \qquad + B_1V_i, (nT, d_nT) \qquad \text{switch on} \\ \dot{X} = A_2X \\ \qquad + B_2V_i, (d_nT, (n+1)T) \quad \text{switch off}, \end{cases} \qquad (27)$$

where, $A_1 = \begin{bmatrix} -\frac{1}{RC} & 0 \\ 0 & 0 \end{bmatrix}$, $A_2 = \begin{bmatrix} -\frac{1}{RC} & \frac{1}{C} \\ -\frac{1}{L} & 0 \end{bmatrix}$, $B_1 = B_2 = \begin{bmatrix} 0 \\ \frac{1}{L} \end{bmatrix}$.

So, for a whole period, during the switch on time and switch off time:

$$\begin{cases} X(d_nT) = e^{A_1d_nT}X(nT) \\ \qquad + \int_{nT}^{(n+d_n)T} e^{A_1((n+d_n)T-\tau)}B_1V_id\tau \\ X((n+1)T) = e^{A_2(1-d_n)T}X(d_nT) \\ \qquad + \int_{(n+d_n)T}^{(n+1)T} e^{A_2((n+1)T-\tau)}B_2V_id\tau. \end{cases} \qquad (28)$$

Then, the relationship of the state variable between nT and $(n+1)T$ can be expressed as:

$$X(nT + T) = N_2N_1X(nT) + [N_2M_1 + M_2]V_i. \qquad (29)$$

In (29), $N_1 = e^{A_1d_nT}$, $N_2 = e^{A_2(1-d_n)T}$, $M_1 = \begin{bmatrix} RC(1 - e^{-\frac{d_nT}{RC}}) & 0 \\ 0 & dT \end{bmatrix} B_1$, $M_2 = A_2^{-1}(e^{A_2(1-d_n)T} - I)B_2$.

For the control loop, the duty ratio can be derived by a switching function:

$$S(X_n, d_n) = v_{con} - v_{ramp} = 0. \qquad (30)$$

v_{con} is the control signal generated by PI controller, and v_{ramp} is the value of PWM comparator. In (31), U_H and U_L are the high and low peak value of the PWM wave.

$$\begin{cases} v_{con} = K_p(V_{ref} - v_C(t)) \\ \qquad + \frac{K_p}{T_i}\int_0^{(n+d_n)T}(V_{ref} - v_C(t))dt \\ v_{ramp} = U_L + (U_H - U_L)(t \bmod T). \end{cases} \qquad (31)$$

Base on (29) and (31), the bifurcation diagram of the output voltage is plotted in Fig. 18.

From Fig. 18, it is obvious that the output voltage is stable when K_p is less than 0.0051. With the gradual increase of K_p, the oscillation phenomenon will appear in output voltage, and the region of oscillation is from 0.0051 to 0.006 according to Fig. 18. This region is basically the same with the simulation results, the region of oscillation is from 0.0049 to 0.006, obtained by PSIM. According to the PSIM simulation results with K_p = 0.0049-0.006, the range about the intersection point of the Nyquist curve and real axis is [−1.154, −0.942].

Therefore, the transition interval from stable region to unstable region, i.e. the critical stable range, can be obtained by simulation, traditional Nyquist analysis and the describing function method, respectively, as given in Table 4.

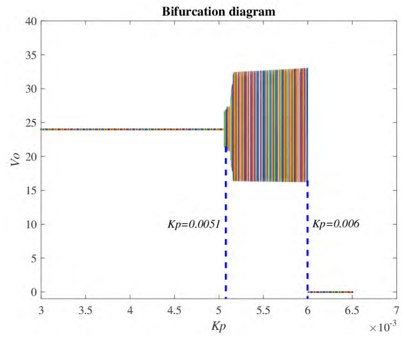

FIGURE 18. The bifurcation diagram of the output voltage with changing K_p.

TABLE 4. The critical stable range determined by simulation, traditional Nyquist and describing function.

Methods	The critical stable range in real axis	The critical stable range of K_p with $T_i = 0.0005$
PSIM Simulation	[-1.154, -0.942]	[0.0049, 0.006]
Traditional Nyquist	[-1]	[0.0052]
Describing Function	[-1.174, -0.97]	[0.0050, 0.0061]

Traditional Nyquist analysis can only determine the critical stable state with a demarcation point. And the transition interval determined by describing function method is close to the circuit simulation result. So the stability analysis based on describing function method is more accurate in the transition interval from stable region to unstable region. And the obtained transition interval can also be regarded as the stability margin for the system.

VIII. CONCLUSION

In this paper, the describing function of PWM switching process has been derived, comparing with the traditional linear modeling and stability analysis method, the critical range of the DC-DC converter system has been extended to a curve, instead of a point $(-1/K, j0)$. The transition interval from stable range to unstable range can be determined exactly by the proposed stability analysis method, which is very helpful for determining the stability margin in real engineering applications. The simulation and experimental results validate the effectiveness and accuracy of the stability analysis based on describing method. Therefore, this paper gives a new choice for the stability analysis of PWM DC-DC converters.

REFERENCES

[1] R. D. Middlebrook, "Small-signal modeling of pulse-width modulated switched-mode power converters," *Proc. IEEE*, vol. 76, no. 4, pp. 343–354, Apr. 1988.
[2] S. Cuk and R. D. Middlebrook, "Advances in switched-mode power conversion Part I," *IEEE Trans. Ind. Electron.*, vol. IE-30, no. 1, pp. 10–19, Feb. 1983.
[3] M. Kumar and R. Gupta, "Stability and sensitivity analysis of uniformly sampled DC-DC converter with circuit parasitics," *IEEE Trans. Circuits Syst. I, Reg. Papers*, vol. 63, no. 11, pp. 2086–2097, Nov. 2016.
[4] M. M. Peretz and S. B. Yaakov, "Time-domain design of digital compensators for PWM DC-DC converters," *IEEE Trans. Power Electron.*, vol. 27, no. 1, pp. 284–293, Jan. 2012.
[5] A. K. Mishra and B. Singh, "Design of PV powered SR motor driven irrigation pumps utilizing boost converter," in *Proc. IEEE Uttar Pradesh Sect. Int. Conf. Elect., Comput. Electron. Eng. (UPCON)*, Dec. 2016, pp. 264–268.
[6] R. D. Middlebrook and S. Cuk, "A general unified approach to modelling switching-converter power stages," in *Proc. IEEE Power Electron. Spec. Conf.*, Jun. 1976, pp. 18–34.
[7] E. Rodriguez, A. El Aroudi, F. Guinjoan, and E. Alarcon, "A ripple-based design-oriented approach for predicting fast-scale instability in DC–DC switching power supplies," *IEEE Trans. Circuits Syst. I, Reg. Papers*, vol. 59, no. 1, pp. 215–227, Jan. 2012.
[8] K. Mehran, D. Giaouris, and B. Zahawi, "Stability analysis and control of nonlinear phenomena in boost converters using model-based Takagi–Sugeno fuzzy approach," *IEEE Trans. Circuits Syst. I, Reg. Papers*, vol. 57, no. 1, pp. 200–212, Jan. 2010.
[9] J. H. B. Deane and D. C. Hamill, "Instability, subharmonics, and chaos in power electronic systems," *IEEE Trans. Power Electron.*, vol. 5, no. 3, pp. 260–268, Jul. 1990.
[10] D. Dai, C. K. Tse, and X. Ma, "Symbolic analysis of switching systems: Application to bifurcation analysis of DC/DC switching converters," *IEEE Trans. Circuits Syst. I, Reg. Papers*, vol. 52, no. 8, pp. 1632–1643, Aug. 2005.
[11] C. K. Tse and M. di Bernardo, "Complex behavior in switching power converters," *Proc. IEEE*, vol. 90, no. 5, pp. 768–781, May 2002.
[12] A. El Aroudi, M. Debbat, R. Giral, G. Olivar, L. Benadero, and E. Toribio, "Bifurcations in DC–DC switching converters: Review of methods and applications," *Int. J. Bifurcation Chaos*, vol. 15, no. 5, pp. 1549–1578, 2005.
[13] A. E. Aroudi, D. Giaouris, H. H. C. Iu, and I. A. Hiskens, "A review on stability analysis methods for switching mode power converters," *IEEE Trans. Emerg. Sel. Topics Circuits Syst.*, vol. 5, no. 3, pp. 302–315, Sep. 2015.
[14] H. Wu, V. Pickert, D. Giaouris, and B. Ji, "Nonlinear analysis and control of interleaved boost converter using real-time cycle to cycle variable slope compensation," *IEEE Trans. Power Electron.*, vol. 32, no. 9, pp. 7256–7270, Sep. 2017.
[15] V. Vorperian, "Simplified analysis of PWM converters using model of PWM switch. II. Discontinuous conduction mode," *IEEE Trans. Aerosp. Electron. Syst.*, vol. 26, no. 3, pp. 490–496, May 1990.
[16] P. T. Krein, J. Bentsman, R. M. Bass, and B. C. Lesieutre, "On the use of averaging for the analysis of power electronic systems," *IEEE Trans. Power Electron.*, vol. 5, no. 2, pp. 182–190, Apr. 1990.
[17] R. W. Erickson, S. Cuk, and R. D. Middlebrook, "Large-signal modelling and analysis of switching regulators," in *Proc. IEEE Power Electron. Spec. Conf.*, Jun. 1982, pp. 240–250.
[18] Y. Ma and K. M. Smedley, "Switching flow-graph nonlinear modeling method for multistate-switching converters," *IEEE Trans. Power Electron.*, vol. 12, no. 5, pp. 854–861, Sep. 1997.
[19] M. Veerachary, "General rules for signal flow graph modeling and analysis of DC-DC converters," *IEEE Trans. Aerosp. Electron. Syst.*, vol. 40, no. 1, pp. 259–271, Jan. 2004.
[20] J. H. Taylor, *Describing Functions*, 1th ed. New York, NY, USA: Wiley, 1999, pp. 6–10.
[21] R. Sridhar, "A general method for deriving the describing functions for a certain class of nonlinearities," *IRE Trans. Autom. Control*, vol. 5, no. 2, pp. 135–141, Jun. 1960.
[22] T. Nabeshima and K. Harada, "Large-signal transient responses of a switching regulator," *IEEE Trans. Aerosp. Electron. Syst.*, vol. AES-18, no. 5, pp. 545–551, Sep. 1982.
[23] Y. Chen, C. K. Tse, S. S. Qiu, L. Lindenmuller, and W. Schwarz, "Coexisting fast-scale and slow-scale instability in current-mode controlled DC/DC converters: Analysis, simulation and experimental results," *IEEE Trans. Circuits Syst. I, Reg. Papers*, vol. 55, no. 10, pp. 3335–3348, Nov. 2008.
[24] J. Li and F. C. Lee, "Modeling of V^2 current-mode control," *IEEE Trans. Circuits Syst. I, Reg. Papers*, vol. 57, no. 9, pp. 2552–2563, Sep. 2009.
[25] S. L. Tian, F. C. Lee, Q. Li, and Y. Y. Yan, "Unified equivalent circuit model of V^2 control," in *Proc. IEEE Appl. Power Electron. Conf. Expo.*, Mar. 2014, pp. 1016–1023.
[26] F. Yu, F. C. Lee, and P. Mattavelli, "A small signal model for V^2 control with composite output capacitors based on describing function approach," in *Proc. IEEE Energy Convers. Congr. Expo.*, Sep. 2011, pp. 1236–1243.

[27] S. Gomariz, F. Guinjoan, E. Vidal-Idiarte, L. Martinez-Salamero, and A. Poveda, ''On the use of the describing function in fuzzy controller design for switching DC-DC regulators,'' in *Proc. IEEE Int. Symp. Circuit Syst.*, May 2000, pp. 247–250.

[28] Y. Qiu, M. Xu, K. Yao, J. Sun, and F. C. Lee, ''Multifrequency small-signal model for buck and multiphase buck converters,'' *IEEE Trans. Power Electron.*, vol. 21, no. 5, pp. 1185–1192, Sep. 2006.

[29] S.-F. Hsiao, D. Chen, C.-J. Chen, and H.-S. Nien, ''A new multiple-frequency small-signal model for high-bandwidth computer V-core regulator applications,'' *IEEE Trans. Power Electron.*, vol. 31, no. 1, pp. 733–742, Jan. 2016.

[30] R. W. Erickson and D. Maksimovic, *Fundamentals of Power Electronics*, 2nd ed. Secaucus, NJ, USA: Kluwer, 2000, ch. 9, pp. 335–337.

[31] H. Li, S. Wang, J. Lü, X. You, and X. Yu, ''Stability analysis of the shunt regulator with nonlinear controller in PCU based on describing function method,'' *IEEE Trans. Ind. Electron.*, vol. 64, no. 3, pp. 2044–2053, Mar. 2017.

[32] K. Ogata, *Modern Control Engineering*, 5th ed. Englewood Cliff, NJ, USA: Prentice-Hall, 2010, ch. 7, pp. 445–450.

[33] S. C. Chung, S. R. Huang, and C. I. Ln, ''Applications of describing functions to estimate the continuous and discontinuous conduction mode for a DC-to-DC buck converter,'' *IEE Proc.-Electr. Power Appl.*, vol. 147, no. 6, pp. 513–519, Nov. 2000.

[34] S. Wang, X. You, H. Li, R. Hao, and T. Q. Zheng, ''Stability analysis of the shunt regulator in PCU with describing function method,'' in *Proc. IEEE Energy Convers. Congr. Expo.*, Sep. 2013, pp. 5385–5389.

[35] J. Shang, H. Li, X. You, T. Q. Zheng, and S. Wang, ''A novel stability analysis approach based on describing function method using for DC-DC converters,'' in *Proc. IEEE Appl. Power Electron. Conf. Expo.*, Mar. 2015, pp. 2642–2647.

[36] D. G. Holmes and T. A. Lipo, *Pulse Width Modulation for Power Converters: Principles and Practice*, 1st ed. Hoboken, NJ, USA: Wiley, 2003, ch. 3, pp. 73–84.

[37] S. S. Bayin, *Essentials of Mathematical Methods in Science and Engineering*, 1st ed. Hoboken, NJ, USA: Wiley, 2008, ch. 11, pp. 510–518.

[38] G. N. Watson, *A Treatise on the Theory of Bessel Functions*, 2nd ed. Cambridge, U.K.: Cambridge Univ. Press, 1966, ch. 3, pp. 38–40.

[39] D. D. Bonar and M. J. Khoury, *Real Infinite Series*, 1st ed. Washington, DC, USA: Mathematical Association of America, 2006, ch. 1, pp. 23–35.

HONG LI (S'07–M'09–S'18) received the B.Sc. degree in electrical engineering from the Taiyuan University of Technology, Taiyuan, China, in 2002, the M.Sc. degree in electrical engineering from the South China University of Technology, Guangzhou, China, in 2005, and the Ph.D. degree in electrical engineering from the University of Hagen, Hagen, Germany, in 2009.

She is currently a Professor with the School of Electrical Engineering, Beijing Jiaotong University, Beijing, China. She has published 1 book, 25 journal papers, and 41 conference papers. She has also applied for 20 patents. Her research interests include nonlinear modeling, analysis and its applications, EMI suppressing methods for power electronic systems, wide-bandgap power devices, and applications.

Dr. Li is an Associate Editor of the IEEE Transactions on Industrial Electronics and the *Chinese Journal of Electrical Engineering*, and the Vice Chairman of the Electromagnetic Compatibility Specialized Committee of China Power Supply Society.

JIANING SHANG received the B.S. and M.S. degrees in electrical engineering from Beijing Jiaotong University, Beijing, China, in 2013 and 2016, respectively.

His research interests include power electronics, nonlinear modeling, and analysis and its applications.

BO ZHANG (M'03–SM'15) was born in Shanghai, China, in 1962. He received the B.S. degree in electrical engineering from Zhejiang University, Hangzhou, China, in 1982, the M.S. degree in power electronics from Southwest Jiaotong University, Chengdu, China, in 1988, and the Ph.D. degree in power electronics from the Nanjing University of Aeronautics and Astronautics, Nanjing, China, in 1994.

He is currently a Professor and the Deputy Dean with the School of Electric Power, South China University of Technology, Guangzhou, China. He has authored or co-authored over 450 papers and 101 patents. He has authored two English monographs in Wiley and one English monograph in Springer. His research interests include nonlinear analysis and control of power supplies and ac drives.

XINGRAN ZHAO received the B.S. degree in electrical engineering from Beijing Jiaotong University, Beijing, China, in 2016, where she is currently pursuing the M.S. degree in electrical engineering.

Her research interests include the modeling and application of wide-bandgap power devices.

NANLIN TAN was born in Nanjing, China, in 1958. He received the B.S. degree from Southwest Jiaotong University in 1982, the M.S. degree from the Nanjing University of Science and Technology in 1987, and the Ph.D. degree from the Nanjing University of Aeronautics and Astronautics, China, in 1994.

He is currently a Professor and a Ph.D. Supervisor with Beijing Jiaotong University, Beijing, China. He is the author or coauthor of more than 100 papers and is the holder of five patents. His research interests include safety technology and engineering, control theory, and pattern recognition.

CHEN LIU received the B.S. degree in electrical engineering from the Wuhan University of Technology, Wuhan, China, in 2017. He is currently pursuing the M.S. degree in electrical engineering with Beijing Jiaotong University, Beijing, China.

His research interests include nonlinear modeling, analysis and its applications.